Adaptive Simulations of Cylindrical Shock Waves in Polytropic van der Waal Gas

Barbara Re(✉), Alessandro Franceschini, and Alberto Guardone

Department of Aerospace Science and Technology, Politecnico di Milano, Milano, Italy
{barbara.re,alberto.guardone}@polimi.it,
alessandro1.franceschini@mail.polimi.it

Abstract. The propagation of converging cylindrical shock waves, collapsing at the axis of symmetry, in a non-ideal gas is investigated by using innovative interpolation-free mesh adaptation techniques. The high pressure, temperature, and energy that can be reached close to the focus point call for thermodynamic models able to take into account the non-ideal gas effects. A distinguishing feature of converging shock waves is the non-constant propagation speed, which makes the flow field behind the shock intrinsically unsteady. To efficiently simulate this configuration, it is fundamental to adapt the computational domain as time evolves. Hence, at each time step, we modify the grid spacing through node insertion, deletion, or relocation according to the current position of the flow features. In this work, any interpolation of the solution between the original and the adapted grids is avoided thanks to a peculiar strategy able to describe mesh adaptation within the arbitrary Lagrangian-Eulerian framework. The adaptive simulation framework, equipped with the polytropic van der Waals equation of state, is assessed first in dilute conditions, where it is possible to compare numerical results with theoretical predictions. In particular, we compute the Guderley-like self-similar solution describing shocks of different intensities propagating in the siloxane MM. Then, it is used to verify the possibility to reach higher energy density when the shock is initiated in the NICFD regime. Finally, we investigate the interaction between the converging shock wave and an arc-shaped obstacle, which is a fundamental phase of the so-called reshaping process, useful to increase the stability of converging shocks.

Keywords: cylindrical shock waves · van der Waals model · mesh adaptation · finite volume scheme

1 Introduction

Converging cylindrical shock waves, collapsing at the axis of symmetry, have been investigated in several theoretical, numerical, and experimental campaigns since the first half of last century [5,7]. Differently from the planar case, converging shocks are intrinsically unsteady phenomena, because the speed of the

M. White et al. (Eds.): NICFD 2022, ERCOFTAC 29, pp. 3–12, 2023.
https://doi.org/10.1007/978-3-031-30936-6_1

shock increases as the radius decreases. Hence, during the propagation towards the focus point, the shock intensity increases, reaching particularly high values of fluid temperature and pressure close to the focus point. The possibility to reach such a high-energy condition has prompted many research activities, motivated by the potential applications in different fields, spanning from medical treatments, e.g., lithotripsy for renal calculi, to power generation, for instance, for the ignition of the nuclear fusion process [1]. Unfortunately, the stability of these flow structures, defined as the capability of the converging wave to approach the cylindrical shape damping out disturbances during the propagation, is of great concern, because small perturbations can make the propagation front deviate from the cylindrical shape [7]. The stability decreases also as the shock Mach number increases. A possible strategy to prevent the onset of instabilities is the so-called *shock-reshaping* process, which turns a cylindrical shock into a prismatic one through controlled reflections. To minimize the possible losses that would reduce the shock intensity, these reflections are generated by lenticular obstacles, i.e., symmetric aerodynamic profiles with sharp leading and trailing edge [6].

The aim of this work is the assessment of a numerical simulation tool for 2D cylindrical converging shocks, without and with obstacles, in non-ideal compressible fluid dynamic regimes, where, for the same pressure jump, higher temperature and energy are reached. The proposed CFD tool performs unsteady inviscid flow simulations using a mesh adaptation strategy, which refines and makes the grid coarser following the shock evolution. Notably, this adaptation is performed within the arbitrary Lagrangian-Eulerian (ALE) framework, so that no interpolation of the solution from the original to the adapted grid is required [2,8]. The siloxane MM is the chosen working fluid for the tests here presented and its thermodynamic behavior is described by the polytropic van der Waals model.

This work represents the first step of a wider project, whose long-term goal is the study of how the obstacle geometry and the fluid dynamic behavior affect the intensity and the stability of the converging shock waves.

2 The Numerical Method

Assuming the flow as inviscid, i.e., neglecting thermal conductivity and viscosity, the fluid flow behavior is described by the unsteady compressible Euler equations. To close the system, the van der Waals equation of state (EOS) is considered:

$$p = \frac{RT}{v - b} - \frac{a}{v^2} \tag{1}$$

where p is the pressure, T the temperature, v the specific volume, R the gas constant, and a and b are the fluid-specific parameters of the van der Waals equation that account for non-ideal gas effects about covolume and intermolecular attractive forces. To a first approximation and to compare numerical results with theoretical predictions, the polytropic assumption is made. So, the value of

the specific heat at constant volume c_v is computed through the Aly-Lee equation [3] at $T = 300$ K, and it is assumed to be constant during the simulation, even though the high temperatures and the low densities that can be reached at the focus point could jeopardize the hypothesis of polytropic gas [12].

2.1 The Unsteady Adaptive Finite Volume Scheme

The governing equations are integrated in space over an unstructured, triangular mesh that discretizes the domain Ω, through a node-centered, edge-based finite volume scheme. The equations are discretized within an ALE framework that allows the finite volumes to move and deform independently from the flow velocity. Thanks to a peculiar three-step procedure, also the topology changes due to mesh adaptation—such as node insertion, node deletion, and edge swapping—are described within a standard ALE formulation [8]. A backward-finite-difference implicit scheme with a dual time-step technique is used as time integrator.

The unsteady adaptive discretization strategy is well-suited for the simulation of the converging shock waves because the mesh can be modified to follow moving flow features: as shown in Fig. 1, the minimum grid spacing is reached only close to the shock wave, increasing the accuracy while keeping the number of grid nodes under control. The adaptation process is driven by criteria based on the derivatives of the flow variables: where large variations are detected, the local grid spacing is reduced, whereas it is enlarged where the solution is smooth, without jeopardizing solution accuracy [9,10]. The adaptation criterion is a weighted combination of the magnitude of the Hessian of the Mach number and the gradient of the density, with weights 0.8 and 0.2, respectively. The same strategy can be used also to follow arbitrarily large displacements of the boundary domain [11], but in this work we consider only a domain with fixed boundaries.

Due to the axial symmetry of the numerical domain, the computational cost is reduced by considering only a slice of the 2D cylinder section. The computational domain, shown in Fig. 1, is thus defined by three boundaries: the lower and the upper walls that merge at the focus point, which are modeled as inviscid walls, and the external boundary shaped as an arc of a circle, where non-reflecting boundary conditions are imposed.

The simulations are initialized with null velocity, and a jump in pressure and density at a certain radial distance (R_0) from the focus point, hence with a radial version of the Riemann problem. The post-shock density is computed according to the Rankine-Hugoniot adiabatic jump relations for a perfect gas, as in [13]. After the diaphragm rupture, a shock wave and a contact discontinuity propagate inward, while a rarefaction fan propagates outward. We remind that, unlike the planar case, the internal, i.e., post-shock, state is time-dependent because the shock intensity increases while converging.

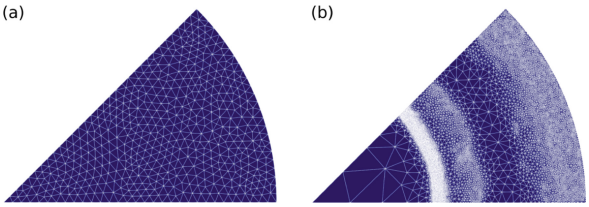

Fig. 1. Computational domain: a) initial grid, with a uniform grid spacing $h_0 = 0.01$ m; b) example of an adapted grid obtained during the simulation. The radial length of the mesh is 0.31 m. During adaptation, the imposed minimum edge size is $h_{\min} = 0.001$ m

2.2 Characterization of Converging Shock Waves

The evolution of cylindrical shock waves can be approximated according to Guderley's law [5]:

$$\frac{R_s}{R_0} = \left(1 - \frac{t}{\tilde{\tau}}\right)^{\alpha}, \tag{2}$$

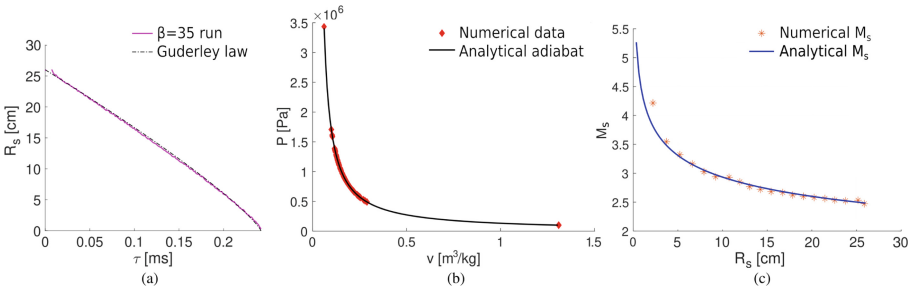

Fig. 2. Comparison of numerical data and theoretical predictions for the MM in dilute conditions, for the $\beta = 35$ case.

which expresses the shock position R_s as function of the time t. R_0 is the initial shock radius and $\tilde{\tau}$ the total focusing time, namely the time required by the shock to reach the focus point. Finally, α is the self-similarity exponent, which is a function of shock geometry (planar, cylindrical, or spherical) and thermodynamics of the gas. For the ideal gas, the theoretical value of α for cylindrical shocks is 0.834, while in this work, the numerical value according to the van der Waals EOS is computed through a non-linear least squares approach with numerical data.

A further theoretical result useful for validation is the post-shock pressure along the Hugoniot adiabatic curve, according to the van der Waals model, which can be defined in the p-v plane as

$$p_2 = p_2(p_1, v_1, v_2) = \left[\frac{1}{\delta_\gamma}\left(p_1 + \frac{a}{v_1^2}\right)(v_2 - b) - \frac{1}{2}p_1(v_2 - v_1) + \frac{a}{v_2\delta_\gamma}\left(\frac{b}{v_2} - 1\right)\right] \Big/ \left[\left(\frac{1}{2} + \frac{1}{\delta_\gamma}\right)v_2 - \left(\frac{v_1}{2} + \frac{b}{\delta_\gamma}\right)\right], \quad (3)$$

where $\delta_\gamma = R/c_v$, and the subscripts 1 and 2 refer to the pre- and post-shock state, respectively.

Finally, the monotonic behavior of the shock front intensity is evaluated by computing the shock Mach number as a function of the shock radius. To do so, Guderley's law is derived with respect to time as:

$$M_S^G(t_k) = \frac{1}{c_1} \cdot \left|\frac{\partial R_s(t_k)}{\partial t}\right|_{t_k} = \frac{R_s \cdot \alpha}{c_1 \cdot (\tilde{\tau} - t_k)}, \quad (4)$$

where c_1 is the pre-shock speed of sound and t_k is the k-th time step.

From the numerical results, we compute the shock position R_s in the radial direction in a post-process step by using an ad-hoc algorithm, devised following the three criteria proposed by Vignati and Guardone [13]. We evaluate the post-shock state through a similar strategy, but, due to the fact the shock wave is represented over more than one cell due to numerical viscosity, it is extracted at a position $R_e \geq R_s$, and R_e is computed by solving a local maximum problem of the second order derivative of the pressure in the proximity of R_s [4].

3 Results

Simulations of converging shock waves with siloxane MM are now presented. Different values of the pressure jump $\beta = p_2/p_1$ across the diaphragm of the numerical Riemann problem are tested. In the first case, we consider $\beta = 35$, with $p_1 = 0.0516\ p_c$ and density $\rho_1 = 0.0039\ \rho_c$, namely in dilute gas conditions (the subscript c indicates critical variables), where a fair agreement with the perfect gas model is expected. The diaphragm is located at $R_0 = 26$ cm, whereas the domain length in the radial direction is 31 cm. The numerical results and the theoretical predictions are compared in Fig. 2. The shock position, in panel (a), is compared with the theoretical Guderley's law with the ideal gas self-similar exponent $\alpha = 0.834$. The fitted value of α results equal to 0.852, deviating about 2% from the ideal gas model case, in these dilute conditions. In Fig. 2(b), post-shock states computed from the numerical simulation are plotted along with the shock adiabatic curve in the $p - v$ plane, observing a good agreement. Starting from the pivot state, namely the one at the highest specific volume, throughout its propagation, the converging shock wave progressively increases the fluid post-shock pressure, eventually attaining values in the order of GPa. The latest comparison for this validation case is the shock Mach number as a

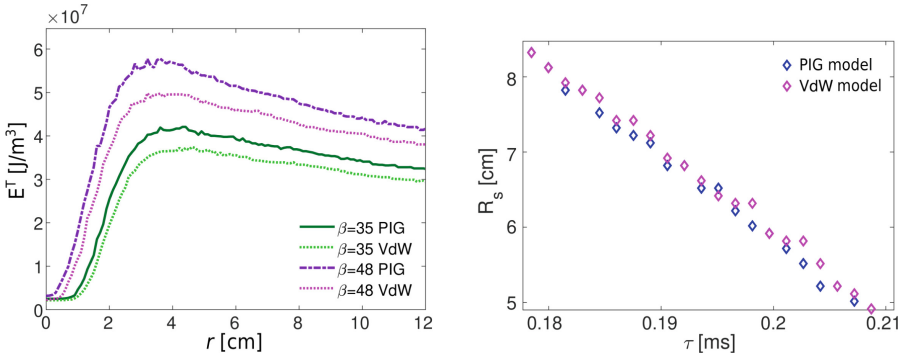

Fig. 3. Comparison between the results for the MM siloxane in dilute conditions, modelled with ideal and van der Waals EOS. Left: total energy close to the focus point; right: shock position close to focus point.

function of shock radius, through Eq. (4), where, again, a good agreement is achieved and the Mach number of the shock front monotonically increases as the shock propagates. More specifically, from Fig. 2(c), it can be seen that the region close to the focus point is characterized by a higher slope of the curve, meaning that the last instants of the convergence process are contributing the most to the increase of fluid energy. This is the reason behind the importance of keeping as stable as possible the shock front during the implosion process in practical applications.

Now, the importance and influence of the selected thermal EOS to model the fluid behavior are assessed, considering the same numerical setup for each test. Tested values of pressure jump are $\beta = 35$ and $\beta = 48$. Relevant fluid dynamics variables are sampled from probes located along a radial coordinate r. Figure 3 (left) shows the differences in the total energy density, at two different time instants, one for each value of β. The differences in energy are important, especially once the converging shock has reached the focus point. Pressure values are lower with van der Waal EOS than with the perfect gas because attractive forces reduce fluid pressure at a given thermodynamic state. Consequently, lower pressure means lower temperature and lower total energy E^T. Moreover, results with the van der Waals model are characterized by larger values of shock radius at a given time, which reflect eventually into Guderley's law. Indeed, looking at the region close to the focus point, reported in Fig. 3 (right), the ideal gas confirms its tendency of overestimating the shock wave speed to the van der Waals model, because, at a given time step, lower values of shock radius are determined by a higher shock wave speed.

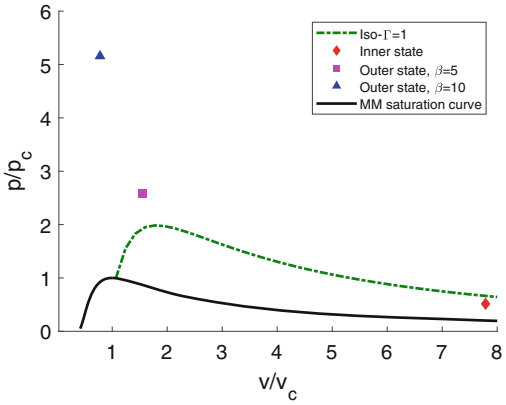

Fig. 4. Initial Riemann problem states for the tests with siloxane MM in NICFD conditions. The saturation curve is drawn in black, along with the isoline at $\Gamma = 1$ that delimits the NICFD region. The red marker denotes the initial, pre-shock, state. The blue and the violet markers depict, respectively, the post-shock state corresponding to $\beta = 5$, and $\beta = 10$, respectively.

Converging shock waves are then simulated in the non-ideal regime, which is bounded by $\Gamma = 1$ iso-line and is characterized by classical gas dynamics features, but the speed of sound dependence on the density is the opposite to the ideal regime. The initial conditions, displayed in Fig. 4, are $p_1 = 0.5157\ p_c$ and $\rho_1 = 0.1284\ \rho_c$, and two values of pressure jumps are simulated, $\beta = 5$ and $\beta = 10$. Shock position in time is depicted in Fig. 5 and it qualitatively agrees with the behavior predicted by Guderley's law. Moreover, the extrapolated power law exponents α computed for the two different β values show a variation lower than 1%, as proof of the validity of the implemented framework.

To evaluate if the compression factor attained in the proximity of the focus point is enhanced due to initial dense working conditions, the behavior of the pressure coefficient trace, defined as $c_p = \frac{p}{p_1}$, is investigated by computing the trace at the first probe (located at $r = 0.001$ m), shown in Fig. 6. As expected, starting from the same pre-shock conditions, higher values of β are associated with lower total focusing time, since the shock wave converges faster. In fact, the trace peak for $\beta = 10$ is reached at an earlier time. Moreover, doubling the pressure jump β, the maximum pressure coefficient value increases from $c_p^{\max} = 42.4$ to $c_p^{\max} = 106.4$, so it increases more than twice. This super-linear proportionality of the pressure coefficient on the pressure jump has been observed only in the non-ideal regime. Hence, working in dense conditions, with an initial condition close to the saturation curve, could lead easier to higher gas energy states at the focus point, which is an aspect of primary importance for practical applications of cylindrical converging shock waves.

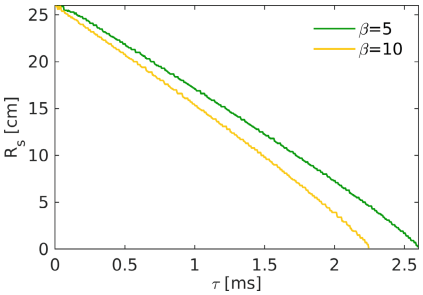

Fig. 5. Guderley's law from numerical simulation of MM siloxane in NICFD conditions.

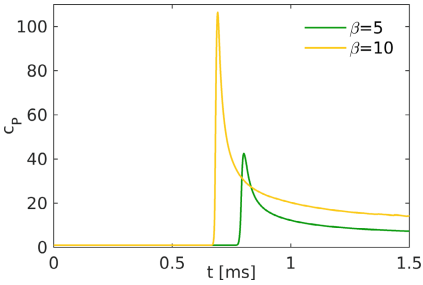

Fig. 6. Pressure coefficient traces in NICFD conditions at $r = 0.001$ m.

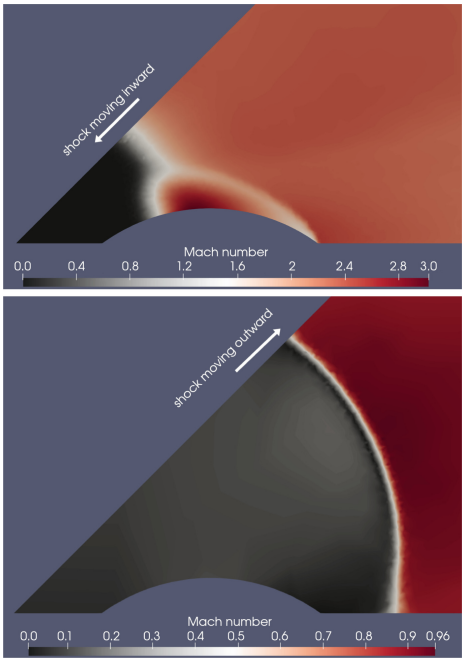

Fig. 7. Mach number contour plots for the test with the obstacle, in dense condition, at a time instant before (top) and after (bottom) the focus time.

Finally, a numerical simulation of a cylindrical converging shock wave that interacts with an obstacle is performed. The obstacle is an arc-shaped profile located in the proximity of the focus point, which generates a truly 2D flow field. Figure 7 (left) shows the Mach reflection caused by the shock-obstacle interaction. This flow structure, composed by the incident shock, the reflected shock and the third shock that travels parallel to the surface called Mach stem, is required to obtain cylindrical shock reshaping, regardless of the reflection type occurring in correspondence with the obstacle leading edge [13]. The robustness of the developed framework for adaptive 2D simulations of cylindrical shock waves has been proven through the computation of the flow field behavior also after the focus point is reached. Figure 7 (right) shows the Mach field when the shock wave has already been reflected at the focus point and passed the obstacle.

4 Conclusions

For the first time, 2D interpolation-free adaptive simulations of cylindrical converging shock waves have been carried out, assessing the validity of an innovative unsteady solver for the ALE formulation of the Euler equations over adaptive

grids in NICFD regimes. The siloxane MM has been modeled through the van der Waals EOS, accounting for non-ideal gas effects. Several initial jump conditions for the radial Riemann problem have been tested, along with the effects of the thermodynamic model. The ideal gas model proved to overestimate the propagation velocity of the converging shock, even in dilute conditions. The simulations in the NICFD regime demonstrated that working in such conditions is efficient to obtain a higher energy state of the gas in close proximity to the focus point. Finally, the ultimate purpose of this work has been about the numerical simulation of a converging shock wave that eventually interacts with an obstacle, undergoing a reshaping process. In practical applications, reshaping into polygonal shocks is exploited since the latter are more stable. Results showed how the numerical method adopted is suitable for this type of problem. The Mach reflection pattern leading to the shock wave reshaping has been simulated. Moreover, the robustness of the method permits to represent properly the flow field once the converging shock wave has reached the focus point and is bounced back, moving outwards the computational domain.

References

1. Clark, D., Tabak, M.: A self-similar isochoric implosion for fast ignition. Nucl. Fusion **47**, 1147–1156 (2007). https://doi.org/10.1088/0029-5515/47/9/011
2. Colombo, S., Re, B.: An ALE residual distribution scheme for the unsteady Euler equations over triangular grids with local mesh adaptation. Comput. Fluids **239**, 105414 (2022). https://doi.org/10.1016/j.compfluid.2022.105414
3. Colonna, P., Nannan, N.R., Guardone, A., Lemmon, E.W.: Multiparameter equations of state for selected siloxanes. Fluid Phase Equilib. **244**, 193–211 (2006). https://doi.org/10.1016/j.fluid.2006.04.015
4. Franceschini, A.: Cylindrical shock waves in high molecular complexity van der Waals fluid. Master's thesis, Politecnico di Milano, July 2022
5. Guderley, K.G.: Stark kugelige und zylindrische verdichtungsstöße in der nähe des kugelmittelpunktes bzw. der zylinderachse. Luftfahrtforschung **19**, 302 (1942)
6. Kjellander, M., Tillmark, N., Apazidis, N.: Thermal radiation from a converging shock implosion. Phys. Fluids **22**(4), 046102 (2010). https://doi.org/10.1063/1.3392769
7. Perry, R.W., Kantrowitz, A.: The production and stability of converging shock waves. J. Appl. Phys. **22**, 878–886 (1951). https://doi.org/10.1063/1.1700067
8. Re, B., Dobrzynski, C., Guardone, A.: An interpolation-free ALE scheme for unsteady inviscid flows computations with large boundary displacements over three-dimensional adaptive grids. J. Comput. Phys. **340**, 26–54 (2017). https://doi.org/10.1016/j.jcp.2017.03.034
9. Re, B., Dobrzynski, C., Guardone, A.: Assessment of grid adaptation criteria for steady, two-dimensional, inviscid flows in non-ideal compressible fluids. Appl. Math. Comput. **319**, 337–354 (2018). https://doi.org/10.1016/j.amc.2017.03.049
10. Re, B., Guardone, A.: An adaptive ALE scheme for non-ideal compressible fluid dynamics over dynamic unstructured meshes. Shock Waves **29**, 73–99 (2019). https://doi.org/10.1007/s00193-018-0840-2

11. Re, B., Guardone, A., Dobrzynski, C.: An adaptive conservative ALE approach to deal with large boundary displacements in three-dimensional inviscid simulations. In: 55th AIAA Aerospace Sciences Meeting, Grapevine, Texas, 9–13 January 2017 (2017). https://doi.org/10.2514/6.2017-1945
12. Vignati, F.: Dynamics of cylindrical converging shock waves interacting with circular-arc obstacles. Ph.D. thesis, Politecnico di Milano (2015)
13. Vignati, F., Guardone, A.: Dynamics of cylindrical converging shock waves interacting with aerodynamic obstacle arrays. Phys. Fluids **27**, 066101 (2015). https://doi.org/10.1063/1.4921680